

# We are IntechOpen, the world's leading publisher of Open Access books Built by scientists, for scientists

6,000

Open access books available

148,000

International authors and editors

185M

Downloads

Our authors are among the

154

Countries delivered to

TOP 1%

most cited scientists

12.2%

Contributors from top 500 universities



WEB OF SCIENCE™

Selection of our books indexed in the Book Citation Index  
in Web of Science™ Core Collection (BKCI)

Interested in publishing with us?  
Contact [book.department@intechopen.com](mailto:book.department@intechopen.com)

Numbers displayed above are based on latest data collected.  
For more information visit [www.intechopen.com](http://www.intechopen.com)



Chapter

# Multi-Metric Near-Optimal Image Denoising

*Kenji Hara and Kohei Inoue*

## Abstract

It is necessary to optimize the parameters for each image input to achieve the maximum denoising performance because the performance of denoising algorithms depends largely on the selection of the associated parameters. The commonly used objective image quality measures in quantitatively evaluating a denoised image are PSNR, SSIM, and MS-SSIM, which assume that the original image exists and is fully available as a reference. However, we do not have access to such reference images in many practical applications. Most existing methods for no-reference denoising parameter optimization either use the estimated noise distribution or a unique no-reference image quality evaluation measure. In the chapter, for BM3D, which is a state-of-the-art denoising algorithm, we introduce a natural image statistics (NIS) based on the generalized Gaussian distribution (GGD) and the elastic net regularization (EN) regression method and propose its use to perform the BM3D parameter optimization for PSNR, SSIM, and MS-SSIM, respectively, which are the popular image quality evaluation measures, without reference image and knowledge of the noise distribution. Experimental results with several images demonstrate the effectiveness of the proposed approach.

**Keywords:** denoising parameter optimization, BM3D, full-reference image quality, Kullback-Leibler divergence, elastic net regularization regression

## 1. Introduction

Image denoising is used for various tasks, such as segmentation, enhancement, frequency decomposition, and local feature extraction. The performance of denoising algorithms generally depends largely on the selection of the parameters. We address the problem of optimizing the parameters of denoising algorithms to achieve maximum performance. The most common image quality evaluation metrics used to quantitatively evaluate the performance of denoising methods include full-reference metrics such as peak signal-to-noise ratio (PSNR), structural similarity index measure (SSIM) [1], and multi-scale structural similarity index measure (MS-SSIM) [2], which assume that the original image exists and is fully available as a reference. However, such reference images are not available in many practical applications. Therefore, no-reference image denoising approaches have been intensively developed.

Several methods for optimizing denoising parameters without reference have been proposed that use cross-validation [3, 4] and the L-curve method [5, 6]. These methods are somewhat empirical and hence not necessarily optimization methods in the strict sense. Subsequently, a class of parameter optimization methods [7–9] was developed to minimize an estimate of the mean-squared error (MSE) obtained using Stein’s unbiased risk estimate (SURE) [10]. This approach performs PSNR optimization without requiring a reference. Although PSNR is not necessarily a good evaluation measure of image quality, it remains among the most popular objective image quality metrics. However, this SURE-based approach generally necessitates the accurate estimation of the noise variance in the noisy image, which is not trivial.

Recently, Zhu et al. [11] proposed a no-reference optimization method based on a perceptual and no-reference image quality evaluation metric, which requires no knowledge of the noise distribution. Their image quality evaluation metric is very interesting in itself, but is not necessarily widely used. To the best of knowledge, most existing methods for no-reference denoising parameter optimization either use the estimated image noise or individual no-reference image quality evaluation metrics. The only exception is the no-reference parameter optimization method by D’Elia et al. [12], which requires no estimation of noise statistics and achieves its optimality only under the SSIM metric. However, PSNR and MS-SSIM metrics are also widely used for the assessment of image quality. Thus, a denoising algorithm to guarantee the near-optimality with respect to the non-SSIM criterion, particularly for PSNR and MS-SSIM, is proposed in this chapter. The proposed framework can also easily be extended to incorporate any full-reference image quality measurement metrics that might be discovered in the future.

In the chapter, we propose a novel technique for no-reference parameter optimization in the BM3D denoising algorithm, which is the current state-of-the-art denoising method. Our method adaptively depends on which of the following most widely used full-reference image quality evaluation metrics is optimized: PSNR, SSIM, and MS-SSIM, and requires no knowledge of the noise distribution. To do so, we introduce a natural image statistics (NIS) model based on the generalized Gaussian distribution (GGD) and an elastic net regularization regression model. The pipeline of our method is illustrated in **Figure 1**. Experimental results using SIDBA images are presented to show the effectiveness of the proposed method.

The remainder of chapter is organized as follows. In Section 2, we describe a statistical model of natural images in the wavelet transform domain. In Section 3, we formulate a minimization problem of a statistical distance measure to estimate the optimal parameters under the SSIM and MS-SSIM metrics. In Section 4, we derive a regression-based bias correction procedure to estimate the optimal parameter under the PSNR metric by refining a quasi-optimal parameter. In Section 5, we

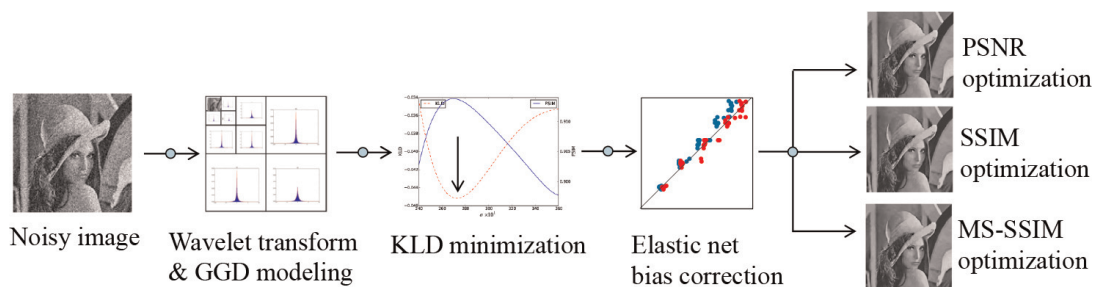


**Figure 1.**  
Pipeline of our method.

present experimental results obtained by applying the proposed framework to each state-of-the-art denoising method. Section 5 concludes the chapter.

## 2. Statistical model of natural images

In this section, we use a slight modification of Mallat's statistical model of natural images [13] based on generalized Gaussian modeling in the wavelet transform domain. The generalized Gaussian distribution (GGD) [14] refers to a family of symmetric distributions, which includes the Gaussian, the Laplacian, and the uniform distributions as special cases. Recently, GGD has been successfully used in the fields of pattern recognition and image processing, in applications such as texture retrieval [15], digital watermarking [16], face recognition [17], and image segmentation [18–20].

The probability density function (pdf) of GGD with a mean zero is given by

$$p(x; \alpha, \beta) = \frac{\beta}{2\alpha\Gamma(1/\beta)} e^{-|x/\alpha|^\beta}, \quad (1)$$

where  $\alpha$  and  $\beta$  are, respectively, the scale and shape parameters (GGD parameters) and  $\Gamma(z) = \int_0^\infty e^{-t} t^{z-1} dt$  ( $z > 0$ ) is the gamma function. For  $\beta = 2$ , Eq. (2) is equivalent to the Gaussian distribution, whereas for  $\beta = 1$ , it is equivalent to the Laplace distribution. When  $\beta \rightarrow 0+$ , Eq. (2) becomes a Dirac delta function distribution, and when  $\beta \rightarrow +\infty$ , the distribution converges to a uniform distribution, as shown in **Figure 2**, and when  $\beta \rightarrow +\infty$ , the distribution converges to a uniform distribution. The maximum-likelihood estimation (MLE) [21, 22], moment-based [23], and global convergence (GCM) [24] methods are widely used to estimate the GGD parameters ( $\alpha, \beta$ ). As described below, a statistical feature for natural image is described as a set of the estimated parameters of GGD from the marginal distribution of multiresolution wavelet coefficients of a given set of training images [25].

In the proposed approach, we first acquire a large number ( $K$ ) of grayscale natural images. We first apply the discrete wavelet transformation (DWT) to each component image to decompose it into high-pass subbands (SB) of three different frequency levels and three different orientations, including horizontal subbands  $\{H_j\}_{j=1,2,3}$ ,

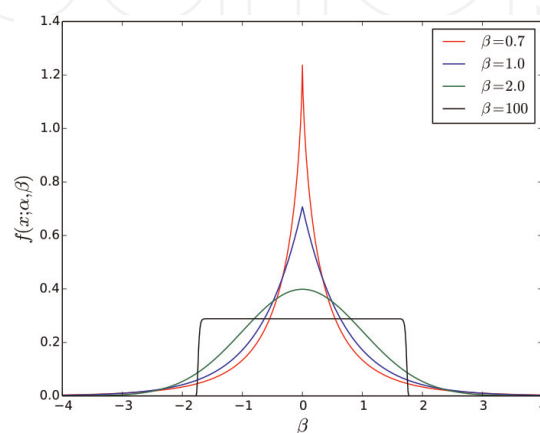


**Figure 2.**  
 The probability density functions of generalized Gaussian distribution with different shape parameters  $\beta$ .

vertical subbands  $\{V_j\}_{j=1,2,3}$ , diagonal subbands  $\{D_j\}_{j=1,2,3}$ , and low-pass subbands  $A_3$ , where  $j = 1,2,3$  denotes the resolution level of the DWT. Then, for each of the  $9 (= 3 \times 3)$  high-pass subband components  $\left\{ \{G_j\}_{G=H,V,D} \right\}_{j=1,2,3}$ , of each image, we generate a normalized histogram (SB histogram) with a bin width  $h = 3.5s/n^{1/3}$ , where  $n$  is the number of pixels and  $s$  is the standard deviation of the pixel values, using Scott's rule [26]. For each of the 9 SB histograms of each image, we estimate the GGD parameters  $\left\{ \left\{ \hat{\alpha}_{G_j}^{(k)}, \hat{\beta}_{G_j}^{(k)} \right\}_{G=H,V,D} \right\}_{j=1,2,3}$ , by the MLE method [21, 22], where  $k = 1, \dots, K$  is the image number. Finally, as a learning result from natural images, we obtain a set of GGDs for the 9 SB components whose pdfs are given by

$$p_{G_j}(x) = f\left(x; \bar{\alpha}_{G_j}, \bar{\beta}_{G_j}\right), \quad (2)$$

where  $f(\cdot; \cdot, \cdot)$  is the pdf of GGD defined by Eq. (2).  $\bar{\alpha}_{G_j}$  and  $\bar{\beta}_{G_j}$  are respectively the mean values of the total number  $K$  of the estimated  $\alpha$  and  $\beta$  parameters for each SB component; that is,

$$\bar{\alpha}_{G_j} = \frac{1}{K} \sum_{k=1}^K \hat{\alpha}_{G_j}^{(k)}, \quad \bar{\beta}_{G_j} = \frac{1}{K} \sum_{k=1}^K \hat{\beta}_{G_j}^{(k)}. \quad (3)$$

### 3. Parameter quasi-optimization

In the study, we address the problem of optimizing the parameters of the BM3D algorithm (block-matching and 3D filtering) [27]. The BM3D algorithm is designed to denoise images corrupted with zero-mean additive Gaussian noise. A modified version called SAR-BM3D has also been proposed, which assumes multiplicative speckle noise.

Firstly, the algorithm divides a noisy image into blocks. The similar blocks are stacked together to form a 3D array. Then, based on the structural similarity in each group, collaborative filtering and weighted averaging are carried out. The BM3D algorithm requires that an associated parameter  $\sigma$  be set to the noise variance of the image. However, accurate estimation of the noise distribution present in an image is not trivial. In addition, such an optimal denoising parameter generally varies depending on the selection of evaluation criteria.

Here, we consider that the quasi-optimal parameter  $\bar{\sigma}$  is obtained as the value of  $\sigma$  selected such that a statistical difference between the set of SB histograms of the denoised image using BM3D algorithm and the set of GGD pdfs is minimized. We adopt as the Kullback-Leibler divergence (KLD) [28] as one of the most widely used statistical measures. We solve the following optimization problem.

$$\bar{\sigma} = \underset{\sigma}{\operatorname{argmin}} \sum_{j=1}^3 \sum_{G \in \{H, V, D\}} D_{KL}\left(P_{G_j} \parallel Q_{G_j}(\sigma)\right), \quad (4)$$

where  $D_{KL}\left(P_{G_j} \parallel Q_{G_j}(\Theta)\right)$  denotes the KLD between two distributions  $P_{G_j}$  and  $Q_{G_j}(\Theta)$  as

$$D_{KL}(P_{G_j} \| Q_{G_j}(\sigma)) = \sum_i p_{G_j}(x_i) \log \frac{p_{G_j}(x_i)}{Q_{G_j}(i|\sigma)}, \quad (5)$$

where  $x_i$  and  $Q_{G_j}(i|\sigma)$  ( $G = H, V, D; j = 1, 2, 3$ ) are the center and the value of the  $i$ -th bin in each SB histogram of the denoised image using BM3D algorithm, respectively.  $p_{G_j}(\cdot)$  ( $G = H, V, D; j = 1, 2, 3$ ) is the GGD pdfs defined in Eq. (3).

However, the quasi-optimal parameter  $\bar{\sigma}$  did not necessarily achieve an optimal denoising in some evaluation criteria. Thus, we used a paired  $t$  test at a significance level of  $\alpha = 0.05$ , to determine whether there was a statistically significant difference between the quasi-optimal parameter  $\bar{\sigma}$  and each of  $\sigma_{\text{PSNR}}^*$ ,  $\sigma_{\text{SSIM}}^*$ , and  $\sigma_{\text{MS-SSIM}}^*$ , which denote the ground-truth optimal parameters for the popular image quality evaluation metrics PSNR, SSIM, and MS-SSIM, respectively. As described in Section 5, our experimental results suggest that there is a statistically significant difference in only PSNR between the quasi-optimal and ground-truth optimal parameters. Thus, hereinafter we assume that both of the estimated SSIM-optimal parameter  $\hat{\sigma}_{\text{SSIM}}$  and the estimated MS-SSIM-optimal one  $\hat{\sigma}_{\text{MS-SSIM}}$  are given by the quasi-optimal parameter  $\bar{\sigma}$  and that there was a bias between the ground-truth PSNR-optimal parameter  $\sigma_{\text{PSNR}}^*$  and  $\bar{\sigma}$ . In the next section, we describe a method to correct the bias to obtain the estimated PSNR-optimal parameter  $\hat{\sigma}_{\text{PSNR}}$ .

#### 4. Regression-based bias correction

We generate  $N$  training pairs of noisy and noise-free images by adding zero-mean Gaussian noise of different levels of noise variance and different random seed numbers to original images. Let  $(y_i)_{\text{PSNR}}$  ( $i = 1, \dots, N$ ) (the subscript PSNR is omitted henceforth for brevity) be the objective variable that is the ground-truth PSNR-optimal parameter  $\sigma_{\text{PSNR}}^*$  for the  $i$ -th training pair. Let  $\mathbf{x}_i = (x_i, x_i^2, \dots, x_i^p)^T$  ( $i = 1, \dots, N$ ) be the explanatory variable vector, where  $x_i$  is the estimated quasi-optimal parameter  $\bar{\sigma}$  from the  $i$ -th noisy image. Let  $(\xi_0, \boldsymbol{\xi})_{\text{PSNR}}$  be the regression parameter, where  $\xi_0 \in \mathbb{R}$  and  $\boldsymbol{\xi} = (\xi_1, \xi_2, \dots, \xi_p)^T \in \mathbb{R}^p$ .

Ordinary least squares regression is commonly used to perform polynomial regression. Least squares regression is a simple method, but it is widely known that a more stable and interpretable solution is obtained by incorporating regularization into the solution of ordinary least squares. In such regularization regression models, lasso regression is a typical and well-known approach to impose a L1 norm penalty [29]. However, if there are training samples with high correlation as the noisy training images in our learning system, lasso tends to select only one sample and ignore others. Therefore, the bias correction described in this section is achieved with an elastic net [30], which is a robust regression model and avoids this problem. Using the elastic net regularization regression, the regression parameter is obtained by solving the following optimization problem.

$$\left\{ \hat{\xi}_0, \hat{\boldsymbol{\xi}} \right\} = \underset{(\xi_0, \boldsymbol{\xi}) \in \mathbb{R}^{p+1}}{\operatorname{argmin}} \sum_{i=1}^N (y_i - \xi_0 - \mathbf{x}_i^T \boldsymbol{\xi})^2 + P_\lambda(\boldsymbol{\xi}), \quad (6)$$

where the regularization term  $P_\lambda(\xi)$  is expressed as a linear combination of the L1 norm  $\|\xi\|_1$  and the L2 norm  $\|\xi\|_2^2$  as

$$P_\lambda(\xi) = \lambda_1 \|\xi\|_1 + \lambda_2 \|\xi\|_2^2 = \lambda_1 \sum_{j=1}^p |\xi_j| + \lambda_2 \sum_{j=1}^p \xi_j^2, \quad (7)$$

where  $\lambda_1$  and  $\lambda_2$  are the positive magnitudes of the L1 and L2 norm penalties, respectively. By using the solutions of Eq. (7), the estimated PSNR-optimal parameter  $\hat{\sigma}_{\text{PSNR}}$  is expressed as follows.

$$\hat{\sigma}_{\text{PSNR}} = \bar{\sigma} + \sum_{j=0}^p \left( \hat{\xi}_j \right)_{\text{PSNR}} \bar{\sigma}^j. \quad (8)$$

Note that for correctness the subscript PSNR is shown explicitly in Eq. (8). In our experiments, we used the degree  $p$  of the polynomial as  $p = 3$  and the tuning parameter  $\lambda$  of the elastic net as  $\lambda_1 = \lambda_2 = 5$ .

## 5. Experimental results

$K = 6000$  training images described in Section 3 were randomly selected from photography websites such as <http://pro.foto.com> and <http://sozaing.com>. All the images were cropped to be the size of  $256 \times 256$  pixels. **Figure 3(a, b, c)** shows the plots of the KLD (red curves, left vertical axes) and PSNR, SSIM and MS-SSIM (blue curves, right vertical axes) for different values of the BM3D parameter  $\sigma$  (horizontal axes) for the Lena image corrupted by Gaussian noise  $N(0, 30)$ , respectively. From **Figure 3**, it may be observed that the quasi-optimal parameter  $\bar{\sigma}$ , which is the value of  $\sigma$  minimizing KLD, was slight smaller than the ground-truth PSNR-optimal parameter  $\sigma_{\text{PSNR}}^*$ , whereas  $\bar{\sigma}$  was almost equal to the ground-truth SSIM-optimal and MS-SSIM-optimal parameters  $\sigma_{\text{SSIM}}^*$  and  $\sigma_{\text{MS-SSIM}}^*$ .

Next, a total of  $50 (= 5 \times 5 \times 2)$  noisy SIDBA images (Lena, Pepper, Airplane, Parrots, and Girl) corrupted by five different zero-mean Gaussian noise  $N(0, \sigma_n)$ , ( $\sigma_n = 10, 20, \dots, 50$ ) for different two seeds of random number generator were prepared as training images, and then, the regularization regression described in Section 4 was applied on the training image set to determine the relationships between the quasi-optimal parameter  $\bar{\sigma}$  and each of the ground-truth optimal parameters  $\sigma_{\text{PSNR}}^*$ ,  $\sigma_{\text{SSIM}}^*$ , and  $\sigma_{\text{MS-SSIM}}^*$ .

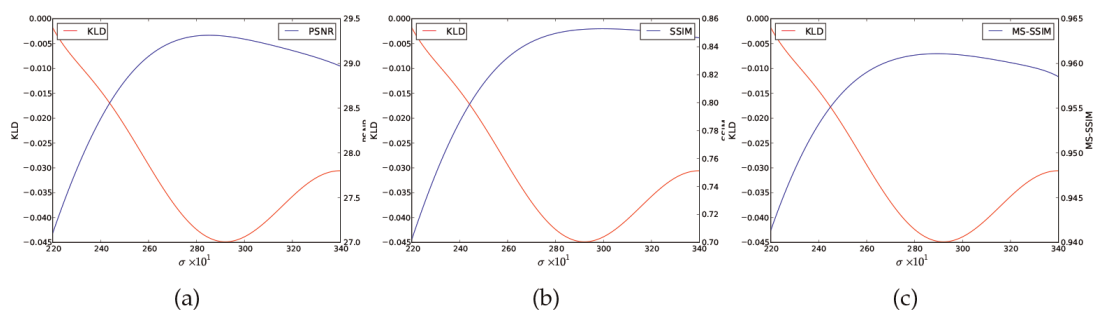


**Figure 3.** Plots of KLD (red curves) and popular image quality evaluation metrics (blue curves) versus different BM3D parameters  $\sigma$ . (a) KLD and PSNR. (b) KLD and SSIM. (c) KLD and MS-SSIM.

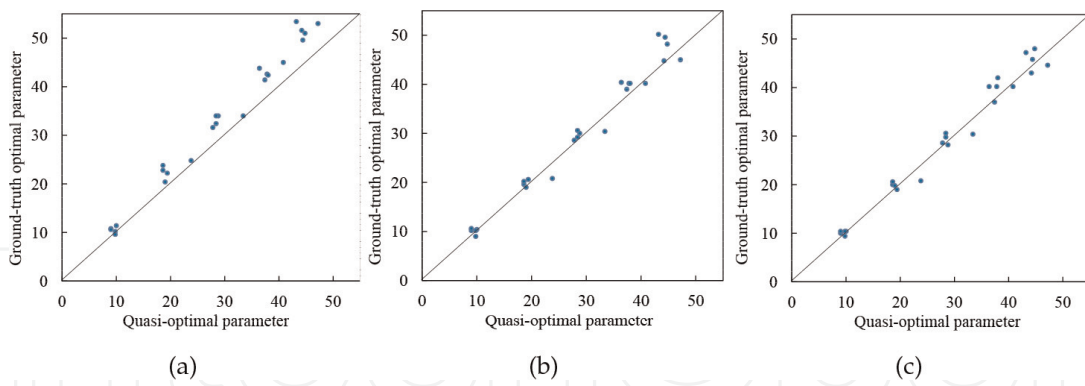


**Figure 4.** Plots of ground-truth optimal parameters versus different quasi-optimal parameters  $\bar{\sigma}$ . (a)  $\sigma_{\text{PSNR}}^*$  versus  $\bar{\sigma}$ . (b)  $\sigma_{\text{SSIM}}^*$  versus  $\bar{\sigma}$ . (c)  $\sigma_{\text{MS-SSIM}}^*$  versus  $\bar{\sigma}$ .

To this end, first we qualitatively evaluated the denoising parameter quasi-optimization described in Section 3. **Figure 4(a, b, c)** shows the plots of the ground-truth optimal parameters  $\sigma_{\text{PSNR}}^*$ ,  $\sigma_{\text{SSIM}}^*$ , and  $\sigma_{\text{MS-SSIM}}^*$  (vertical axes) versus the quasi-optimal parameter  $\bar{\sigma}$  (horizontal axes), respectively. From **Figure 4(a)**, it may be observed that  $\bar{\sigma}$  is smaller than  $\sigma_{\text{PSNR}}^*$  and the trend becomes more significant for larger noise variance. In contrast, from **Figure 4(b, c)**, it may be observed that  $\bar{\sigma}$  was very close to both of  $\sigma_{\text{SSIM}}^*$  and  $\sigma_{\text{MS-SSIM}}^*$ . Furthermore, to quantitatively evaluate the denoising parameter quasi-optimization, we used a paired  $t$  test at a significance level of  $\alpha = 0.05$  to compare the quasi-optimal parameter  $\bar{\sigma}$  with each of the ground-truth optimal parameters  $\sigma_{\text{PSNR}}^*$ ,  $\sigma_{\text{SSIM}}^*$ , and  $\sigma_{\text{MS-SSIM}}^*$ . The results showed no statistically significant differences for SSIM (the paired  $t$  test yielded a  $p$  value of  $0.1167 > 0.05$ ) and MS-SSIM (the paired  $t$  test gives a  $p$  value of  $0.1744 > 0.05$ ), and hence, we estimate the SSIM-optimal and MS-SSIM-optimal parameters as  $\hat{\sigma}_{\text{SSIM}} = \hat{\sigma}_{\text{MS-SSIM}} = \bar{\sigma}$ . In contrast, the above results showed a statistically significant difference for PSNR (the paired  $t$  test gives a  $p$  value of  $5.2962 \times 10^{-8} < 0.05$ ), and thus, we calculated Eq. (8) to find the estimated PSNR-optimal parameter  $\hat{\sigma}_{\text{PSNR}}$ .

To qualitatively evaluate the parameter optimization described in Section 4, we illustrate in **Figure 5(a)** the plots of the ground-truth PSNR-optimal parameter  $\sigma_{\text{PSNR}}^*$  (vertical axis) versus the quasi-optimal parameter  $\bar{\sigma}$  (blue plots, horizontal axis) and the estimated PSNR-optimal parameter  $\hat{\sigma}_{\text{PSNR}}$  (red plots, horizontal axis) for the

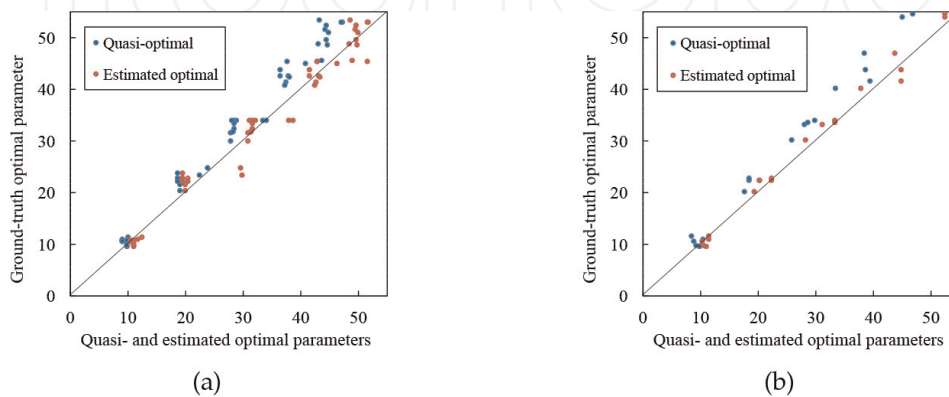


**Figure 5.** Plots of ground-truth PSNR-optimal parameters  $\sigma_{\text{PSNR}}^*$  versus different quasi-optimal parameters  $\bar{\sigma}$  (blue points) and estimated PSNR-optimal parameters  $\hat{\sigma}_{\text{PSNR}}$  (red points) on the training and test image sets. (a) The training image set. (b) The test image set.



training image set. From **Figure 5(a)**, it may be observed that bias correction based on the elastic net regularization regression improved the quasi-optimal parameters. To quantitatively evaluate the parameter optimization described in Section 4, we used a paired  $t$  test at a significance level of  $\alpha = 0.05$  to compare the estimated PSNR-optimal parameter with the ground-truth PSNR-optimal parameter. The results showed no statistically significant differences (the paired  $t$  test gives a  $p$  value of  $p = 0.2692 > 0.05$ ).

In **Tables 1** and **2**, we summarize the pairs of the ground-truth optimal parameters and the metric values and the pairs of the estimated optimal parameters and the

Image	$\sigma_n$	Ground-truth	Estimated	Ground-truth	Estimated	Ground-truth	Estimated
		$(\sigma_{\text{PSNR}}^*, \text{PSNR})$	$(\hat{\sigma}_{\text{PSNR}}, \text{PSNR})$	$(\sigma_{\text{SSIM}}^*, \text{SSIM})$	$(\hat{\sigma}_{\text{SSIM}}, \text{SSIM})$	$(\sigma_{\text{MS-SSIM}}^*, \text{MS-SSIM})$	$(\hat{\sigma}_{\text{MS-SSIM}}, \text{MS-SSIM})$
Lena	10	(10.8, 37.49)	(10.4, 37.48)	(10.2, 0.9950)	(9.0, 0.9946)	(10.0, 0.9930)	(9.0, 0.9927)
	20	(22.8, 35.42)	(19.5, 35.29)	(19.6, 0.9887)	(18.6, 0.9884)	(20.0, 0.9847)	(18.6, 0.9843)
	30	(32.4, 34.35)	(31.6, 34.31)	(29.2, 0.9814)	(28.4, 0.9814)	(29.8, 0.9755)	(28.4, 0.9752)
	40	(42.6, 33.52)	(43.1, 33.52)	(40.2, 0.9722)	(37.8, 0.9715)	(40.2, 0.9644)	(37.8, 0.9611)
	50	(49.6, 32.79)	(49.6, 32.78)	(49.6, 0.9643)	(44.4, 0.9626)	(45.8, 0.9531)	(44.4, 0.9527)
Pepper	10	(11.4, 35.89)	(10.4, 35.88)	(10.4, 0.9930)	(10.0, 0.9930)	(10.4, 0.9917)	(10.0, 0.9916)
	20	(24.8, 34.19)	(25.7, 34.17)	(20.8, 0.9848)	(23.8, 0.9843)	(20.8, 0.9837)	(23.8, 0.9833)
	30	(34.0, 33.46)	(37.8, 33.46)	(30.4, 0.9754)	(33.4, 0.9749)	(30.4, 0.9744)	(33.4, 0.9738)
	40	(45.0, 32.90)	(46.2, 32.89)	(40.2, 0.9638)	(40.8, 0.9636)	(40.2, 0.9631)	(40.8, 0.9630)
	50	(53.0, 32.41)	(51.6, 32.40)	(45.0, 0.9525)	(47.2, 0.9522)	(44.6, 0.9522)	(47.2, 0.9517)
Airplane	10	(10.2, 36.53)	(10.9, 36.53)	(10.2, 0.9635)	(9.8, 0.9634)	(9.4, 0.9903)	(9.8, 0.9902)
	20	(22.2, 35.21)	(20.3, 35.17)	(20.6, 0.9371)	(19.4, 0.9358)	(19.0, 0.9787)	(19.4, 0.9786)
	30	(34.0, 34.51)	(32.0, 34.49)	(30.0, 0.9137)	(28.8, 0.9125)	(28.2, 0.9666)	(28.8, 0.9663)
	40	(41.4, 33.68)	(40.6, 33.66)	(39.0, 0.8893)	(37.4, 0.8884)	(37.0, 0.9529)	(37.4, 0.9529)
	50	(51.6, 32.78)	(50.4, 32.76)	(44.8, 0.8720)	(44.2, 0.8717)	(43.0, 0.9424)	(44.2, 0.9417)
Parrots	10	(10.6, 37.74)	(10.4, 37.73)	(10.6, 0.9889)	(9.0, 0.9873)	(10.4, 0.9905)	(9.0, 0.9897)
	20	(23.8, 35.46)	(20.4, 35.41)	(20.2, 0.9770)	(18.6, 0.9753)	(20.6, 0.9793)	(18.6, 0.9780)
	30	(34.0, 34.46)	(31.5, 34.43)	(30.6, 0.9645)	(28.4, 0.9631)	(30.6, 0.9675)	(28.4, 0.9662)
	40	(42.4, 33.88)	(43.3, 33.86)	(40.2, 0.9512)	(38.0, 0.9462)	(42.0, 0.9549)	(38.0, 0.9475)
	50	(51.0, 33.32)	(50.9, 33.31)	(48.2, 0.9379)	(44.8, 0.9362)	(48.0, 0.9420)	(44.8, 0.9400)
Girl	10	(9.6, 35.53)	(10.9, 35.43)	(9.0, 0.9385)	(9.8, 0.9373)	(10.4, 0.9878)	(9.8, 0.9877)
	20	(20.4, 33.95)	(19.9, 33.94)	(19.0, 0.9044)	(19.0, 0.9044)	(19.8, 0.9742)	(19.0, 0.9741)
	30	(31.6, 33.22)	(30.8, 33.19)	(28.6, 0.8711)	(27.8, 0.8706)	(28.6, 0.9569)	(27.8, 0.9566)
	40	(43.8, 32.74)	(41.4, 32.72)	(40.4, 0.8384)	(36.4, 0.8323)	(40.2, 0.9376)	(36.4, 0.9353)
	50	(53.4, 32.33)	(48.5, 32.32)	(50.2, 0.8066)	(43.2, 0.8046)	(47.2, 0.9179)	(43.2, 0.9177)

**Table 1.**

*Comparison of the ground-truth optimal parameters, the ground-truth metric values, the estimated optimal parameters, and the estimated metric values. The comparisons are shown for the training image set.*

Image	$\sigma_n$	Ground-truth	Estimated	Ground-truth	Estimated	Ground-truth	Estimated
		$(\sigma_{\text{PSNR}}^*, \text{PSNR})$	$(\hat{\sigma}_{\text{PSNR}}, \text{PSNR})$	$(\sigma_{\text{SSIM}}^*, \text{SSIM})$	$(\hat{\sigma}_{\text{SSIM}}, \text{SSIM})$	$(\sigma_{\text{MS-SSIM}}^*, \text{MS-SSIM})$	$(\hat{\sigma}_{\text{MS-SSIM}}, \text{MS-SSIM})$
Balloon	10	(10.6, 38.64)	(10.26, 38.61)	(10.0, 0.9767)	(8.8, 0.9736)	(10.2, 0.9888)	(8.8, 0.9876)
	20	(22.4, 36.54)	(20.2, 36.44)	(19.6, 0.9515)	(18.4, 0.9489)	(20.6, 0.9721)	(18.4, 0.9709)
	30	(33.2, 35.52)	(31.1, 35.46)	(30.2, 0.9287)	(28.0, 0.9254)	(29.6, 0.9533)	(28.0, 0.9520)
	40	(47.0, 34.90)	(43.7, 34.87)	(40.2, 0.9068)	(38.4, 0.8960)	(40.2, 0.9348)	(38.4, 0.9235)
	50	(56.4, 34.36)	(51.7, 34.34)	(48.4, 0.8886)	(45.8, 0.8860)	(48.4, 0.9167)	(45.8, 0.9155)
Couple	10	(9.8, 36.33)	(10.5, 36.29)	(9.2, 0.9303)	(9.2, 0.9303)	(9.6, 0.9872)	(9.2, 0.9871)
	20	(20.2, 33.60)	(19.3, 33.59)	(18.8, 0.8535)	(17.6, 0.8530)	(17.6, 0.9665)	(17.6, 0.9665)
	30	(30.2, 32.66)	(28.2, 32.63)	(27.4, 0.7847)	(25.8, 0.7835)	(26.0, 0.9420)	(25.8, 0.9419)
	40	(40.2, 32.25)	(37.8, 32.22)	(35.6, 0.7216)	(33.4, 0.7199)	(34.0, 0.9157)	(33.4, 0.9154)
	50	(56.8, 32.18)	(49.3, 32.14)	(43.4, 0.6704)	(43.0, 0.6702)	(43.0, 0.8893)	(43.0, 0.8893)
Earth	10	(11.0, 36.26)	(11.4, 36.24)	(10.8, 0.9862)	(10.4, 0.9862)	(10.2, 0.9899)	(10.4, 0.9897)
	20	(22.4, 34.57)	(22.3, 34.57)	(20.6, 0.9711)	(20.2, 0.9709)	(17.4, 0.9759)	(20.2, 0.9742)
	30	(34.0, 33.74)	(33.3, 33.74)	(31.0, 0.9551)	(29.8, 0.9549)	(27.0, 0.9582)	(29.8, 0.9557)
	40	(41.6, 33.11)	(44.8, 33.09)	(40.2, 0.9405)	(39.4, 0.9351)	(34.0, 0.9347)	(39.4, 0.9295)
	50	(54.6, 32.55)	(52.4, 32.53)	(47.2, 0.9257)	(46.8, 0.9256)	(43.0, 0.9191)	(46.8, 0.9141)
Barbara	10	(11.6, 37.40)	(11.4, 37.38)	(10.8, 0.9702)	(8.4, 0.9599)	(10.8, 0.9951)	(8.4, 0.9940)
	20	(22.8, 35.26)	(22.3, 35.25)	(21.0, 0.9396)	(18.4, 0.9324)	(21.4, 0.9872)	(18.4, 0.9862)
	30	(33.6, 34.24)	(33.3, 34.23)	(30.4, 0.9029)	(28.6, 0.9756)	(30.4, 0.9761)	(28.6, 0.9557)
	40	(43.8, 33.81)	(44.8, 33.79)	(40.2, 0.8717)	(38.6, 0.8462)	(40.2, 0.9662)	(38.6, 0.9578)
	50	(54.0, 33.33)	(52.4, 33.32)	(46.8, 0.8374)	(45.0, 0.8348)	(45.8, 0.9532)	(45.0, 0.9530)

**Table 2.**

Comparison of the ground-truth optimal parameters, the ground-truth metric values, the estimated optimal parameters, and the estimated metric values. The comparisons are shown for the test image set.

metric values for different levels of zero-mean Gaussian noise variance and different metrics for the training image set and a test image set consisting of four SIDBA images (Balloon, Couple, Earth, and Barbara; hereinafter are referred to as “the testing image set”), respectively.

In **Figure 5(b)**, we show the plots of the ground-truth PSNR-optimal parameter (vertical axis) versus the quasi-optimal parameter (blue plots, horizontal axis) and the estimated PSNR-optimal parameter (red plots, horizontal axis) for the test image set. From **Figure 5(b)**, as well as the results in **Figure 5(a)**, our bias correction visually improves the quasi-optimal parameters. As in **Figure 5(a)**, we used a paired  $t$  test at a significance level of  $\alpha = 0.05$  to compare the estimated PSNR-optimal parameter with the ground-truth PSNR-optimal parameter. The results showed no statistically significant differences (the paired  $t$  test gives a  $p$  value of  $p = 0.1920 > 0.05$ ), and hence, we can confirm the validity of  $\hat{\sigma}_{\text{PSNR}}$ .

**Figure 6** illustrates a visual comparison of the denoising results. **Figure 6(a)** shows the standard Barbara image. **Figure 6(b)** shows the enlarged detail in the eye



**Figure 6.**

Visual comparison of denoising results. (a) Barbara image. (b) Enlarged detail of (a). (c) Image corrupted by Gaussian noise  $N(0, \sigma_n = 30)$ . (d) Enlarged detail of (c). (e) Denoised image with the BM<sub>3</sub>D algorithm the parameter  $\sigma$  of which is the estimated noise variance from (c) ( $\hat{\sigma}_n = 20.6$ ). (f) Denoised image with the BM<sub>3</sub>D algorithm the parameter  $\sigma$  of which is the estimated PSNR-optimal parameter  $\hat{\sigma}_{\text{PSNR}} = 33.3$ . (g) Denoised image with the BM<sub>3</sub>D algorithm the parameter  $\sigma$  of which is the estimated SSIM-optimal parameter  $\hat{\sigma}_{\text{SSIM}} = 28.6$ . (h) Denoised image with the BM<sub>3</sub>D algorithm the parameter  $\sigma$  of which is the estimated MS-SSIM-optimal parameter  $\hat{\sigma}_{\text{MS-SSIM}} = 28.6$ . (i) Enlarged detail of (e). (j) Enlarged detail of (f). (k) Enlarged detail of (g). (l) Enlarged detail of (h).

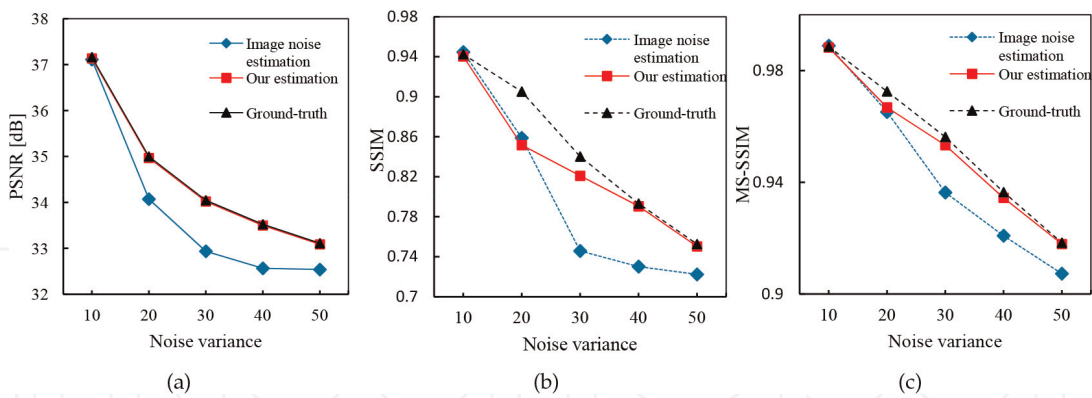


**Figure 7.** Plots of image quality evaluation metric values versus different levels of image noise variance for the direct estimation of the image noise variance (blue lines and points), our proposed method (red lines and points), and the ground-truth (black lines and points). The comparisons are shown for the test image set. (a) PSNR. (b) SSIM. (c) MS-SSIM.

area of the original Barbara image shown in (a). **Figure 6(c)** shows the noisy Barbara image corrupted by additive zero-mean Gaussian noise  $N(0, \sigma_n = 30)$ . **Figure 6(d)** shows an enlarged detail in (c). **Figure 6(e)** shows the denoised image by the BM3D with the directly estimated noise variance from the noisy Barbara image shown in (c) as the parameter value. **Figure 6(f, g, h)** shows the denoised images by the BM3D with the estimated PSNR-optimal, SSIM-optimal and MS-SSIM-optimal parameters, respectively. **Figure 6(i-l)** shows the enlarged details in (e), (f), (g), and (h), respectively. These results indicate that the BM3D model was able to denoise the noisy image with reasonable accuracy by using our estimated optimal parameters.

Finally, for each of the image quality evaluation metrics PSNR, SSIM, and MS-SSIM, we compare the measure value of the BM3D denoised image using our estimated optimal parameters, against that using the estimated noise variance from the input noisy image. **Figure 7(a, b, c)** shows the plots of the mean values of PSNR, SSIM, and MS-SSIM at each noise variance across the test image set, respectively. From these results, it may be observed that the BM3D algorithm with our estimated optimal parameter outperformed that with the directly estimated noise variance from the input images.

## 6. Conclusions

We addressed the problem of estimating the optimal parameter of state-of-the-art denoising algorithm BM3D algorithm without any reference and without any knowledge of the noise distribution, adaptively depending on which of the following widely used image quality evaluation metrics are optimized: PSNR, SSIM, and MS-SSIM. The proposed method for SSIM and MS-SSIM optimization is formulated as a minimization problem for a Kullback-Leibler divergence measure based on the natural image statistics and generalized Gaussian distribution based prior. The method for PSNR optimization is formulated as a combination of the above optimization and an elastic net regression, which provides a very robust regression model. From our experimental results, we have confirmed that the proposed statistical measure and robust regression approach can be used to optimize the denoising parameter of the BM3D algorithm.

IntechOpen

IntechOpen

### **Author details**


Kenji Hara<sup>\*†</sup> and Kohei Inoue<sup>†</sup>  
Department of Media Design, Kyushu University, Fukuoka, Japan

\*Address all correspondence to: [hara@design.kyushu-u.ac.jp](mailto:hara@design.kyushu-u.ac.jp)

† These authors contributed equally.

### **IntechOpen**

---

© 2022 The Author(s). Licensee IntechOpen. This chapter is distributed under the terms of the Creative Commons Attribution License (<http://creativecommons.org/licenses/by/3.0>), which permits unrestricted use, distribution, and reproduction in any medium, provided the original work is properly cited. 

## References

- [1] Wang Z, Bovik AC, Sheikh H, Simoncelli EP. Image quality assessment: From error visibility to structural similarity. *IEEE Transactions on Image Processing*. 2004;**13**(4):600-612. DOI: 10.1109/TIP.2003.819861
- [2] Wang Z, Simoncelli EP, Bovik AC. Multi-scale structural similarity for image quality assessment. In: *Proceedings of the 37th IEEE Asilomar Conference on Signals, Systems & Computers*; 9-12 November 2003. Pacific Grove, CA, USA: IEEE; 2003. pp. 1398-1402
- [3] Golub GH, Heath M, Wahba G. Generalized cross-validation as a method for choosing a good ridge parameter. *Technometrics*. 1979;**21**(2):215-223. DOI: 10.1080/00401706.1979.10489751
- [4] Girard DA. The fast Monte Carlo cross validation and  $C_L$  procedures: Comments, new results and application to image recovery problems. *Computational Statistics*. 1995;**10**: 205-258
- [5] Hansen PC. Analysis of discrete ill-posed problems by means of the L-curve. *SIAM Review*. 1992;**34**(4):561-580. DOI: 10.1137/1034115
- [6] Hansen PC, O'Leary DP. The use of the L-curve in the regularization of discrete ill-posed problems. *SIAM Journal on Scientific Computing*. 1993; **14**(6):1487-1503. DOI: 10.1137/0914086
- [7] Blu T, Luisieri F. The sure-let approach to image denoising. *IEEE Transactions on Image Processing*. 2007; **16**(11):2778-2786. DOI: 10.1109/TIP.2007.906002
- [8] Luisier F, Blu T, Unser M. A new SURE approach to image denoising: Interscale orthonormal wavelet thresholding. *IEEE Transactions on Image Processing*. 2007;**16**(3):593-606. DOI: 10.1109/TIP.2007.891064
- [9] Ramani S, Blu T, Unser M. Monte-Carlo SURE: A black-box optimization of regularization parameters for general denoising algorithms. *IEEE Transactions on Image Processing*. 2008;**17**(9): 1540-1554. DOI: 10.1109/TIP.2008.2001404
- [10] Stein C. Estimation of the mean of a multivariate normal distribution. *Annals of Statistics*. 1981;**9**(6):1135-1151. DOI: 10.1214/AOS/1176345632
- [11] Zhu X, Milanfar P. Automatic parameter selection for denoising algorithms using a no-reference measure of image content. *IEEE Transactions on Image Processing*. 2010;**19**(12): 3116-3132. DOI: 10.1109/TIP.2010.2052820
- [12] D'Elia M, De Los Reyes JC, Miniguano-Trujillo A. Bilevel parameter learning for nonlocal image denoising models. *Journal of Mathematical Imaging and Vision*. 2021;**63**(6):753-775. DOI: 10.1007/s10851-021-01026-2
- [13] Mallat SG. A theory for multiresolution signal decomposition: The wavelet representation. *IEEE Transactions on Pattern Analysis and Machine Intelligence*. 1989;**11**(7): 674-693. DOI: 10.1109/34.192463
- [14] Box GEP, Tiao GC. *Bayesian Inference in Statistical Analysis*. Chichester: John Wiley & Sons; 1997. DOI: 10.1002/9781118033197
- [15] Do MN, Vetterli M. Wavelet-based texture retrieval using generalized

Gaussian density and Kullback-Leibler distance. *IEEE Transactions on Image Processing*. 2002;**11**(2):146-158. DOI: 10.1109/83.982822

[16] Zhu X, Milanfar P. Automatic parameter selection for denoising algorithms using a no-reference measure of image content. *IEEE Transactions on Image Processing*. 2010;**19**(12):3116-3132. DOI: 10.1109/TIP.2010.2052820

[17] Jimenez DG, Gonzalez FP, Alfaro PC, Freire LP, Castro JLA. Modeling Gabor coefficients via generalized Gaussian distributions for face recognition. In: *Proceedings of IEEE International Conference on Image Processing (ICIP2007)*; 16-19 September 2007. San Antonio, TX, USA: IEEE; 2007. pp. IV-485-IV-488

[18] Allili MS, Bouguila N, Ziou D. Finite generalized Gaussian mixture modeling and applications to image and video foreground segmentation. In: *Proceedings of the IEEE Fourth Canadian Conference on Computer and Robot Vision (CRV 07)*; 28-30 May 2007. Montreal, Canada: IEEE; 2007. pp. 183-190

[19] Bazi Y, Bruzzone L, Melgani F. Image thresholding based on the EM algorithm and the generalized Gaussian distribution. *Pattern Recognition*. 2007; **40**(2):619-634. DOI: 10.1016/j.patcog.2006.05.006

[20] Fan S-KS, Lin Y. A fast estimation method for the generalized Gaussian mixture distribution on complex images. *Computer Vision and Image Understanding*. 2009;**113**(7):839-853. DOI: 10.1016/j.cviu.2009.03.003

[21] Joshi RL, Fischer TR. Comparison of generalized Gaussian and Laplacian modeling in DCT image coding. *IEEE*

*Signal Processing Letters*. 1995;**2**(5):81-82. DOI: 10.1109/97.386283

[22] Varanasi MK, Aazhang B. Parametric generalized Gaussian density estimation. *The Journal of the Acoustical Society of America*. 1998;**86**(4):1404-1415. DOI: 10.1121/1.398700

[23] Yu S, Zhang A, Li H. A review of estimating the shape parameter of generalized Gaussian distribution. *The Journal of Computer Information Systems*. 2012;**8**(21):9055-9064

[24] Song KS. A globally convergent and consistent method for estimating the shape parameter of a generalized Gaussian distribution. *IEEE Transactions on Information Theory*. 2006;**52**(2):510-527. DOI: 10.1109/TIT.2005.860423

[25] Morinaga A, Hara K, Inoue K, Urahama K. Classification between natural and graphics images based on generalized Gaussian distributions. *Information Processing Letters*. 2018; **138**:31-34. DOI: 10.1016/j.ipl.2018.05.010

[26] Scott DW. On optimal and data-based histograms. *Biometrika*. 1979; **66**(3):605-610. DOI: 10.2307/2335182

[27] Dabov K, Foi A, Katkovnik V, Egiazarian K. Image denoising by sparse 3D transform-domain collaborative filtering. *IEEE Transactions on Image Processing*. 2007;**16**(8):2080-2095. DOI: 10.1109/TIP.2007.901238

[28] Kullback S, Leibler RA. On information and sufficiency. *The Annals of Mathematical Statistics*. 1951;**22**(1):79-86. DOI: 10.1214/aoms/117729694

[29] Wright J, Yang AY, Ganesh AJ, Sastry SS, Ma Y. Robust face recognition via sparse representation. *IEEE Transactions on Pattern Analysis and*

*Multi-Metric Near-Optimal Image Denoising*  
DOI: <http://dx.doi.org/10.5772/intechopen.106710>

Machine Intelligence. 2009;**31**(2):  
210-227. DOI: 10.1109/TPAMI.2008.79

[30] Zou H, Hastie T. Regularization and  
variable selection via the elastic net.  
Journal of the Royal Statistical Society  
Series B. 2005;**67**(5):301-320. DOI:  
10.1111/j.1467-9868.2005.00527.x

IntechOpen

IntechOpen